**Supporting Information**

# Quantitative Analysis of Thiolated Ligand Exchange on Gold Nanoparticles Monitored by $^1$H NMR Spectroscopy

Ashley M. Smith,[†] Lauren E. Marbella,[†,§] Kathryn A. Johnston,[†,§] Michael J. Hartmann,[†] Scott E. Crawford,[†] Lisa M. Kozycz,[‡] Dwight S. Seferos,[‡] and Jill E. Millstone*[,†]

[†]Department of Chemistry, University of Pittsburgh, 219 Parkman Avenue, Pittsburgh, PA 15260, United States

[‡]Lash Miller Chemical Laboratories, Department of Chemistry, University of Toronto, 80 Saint George Street, Toronto, Ontario M5S 3H6, Canada

**Table of Contents:**

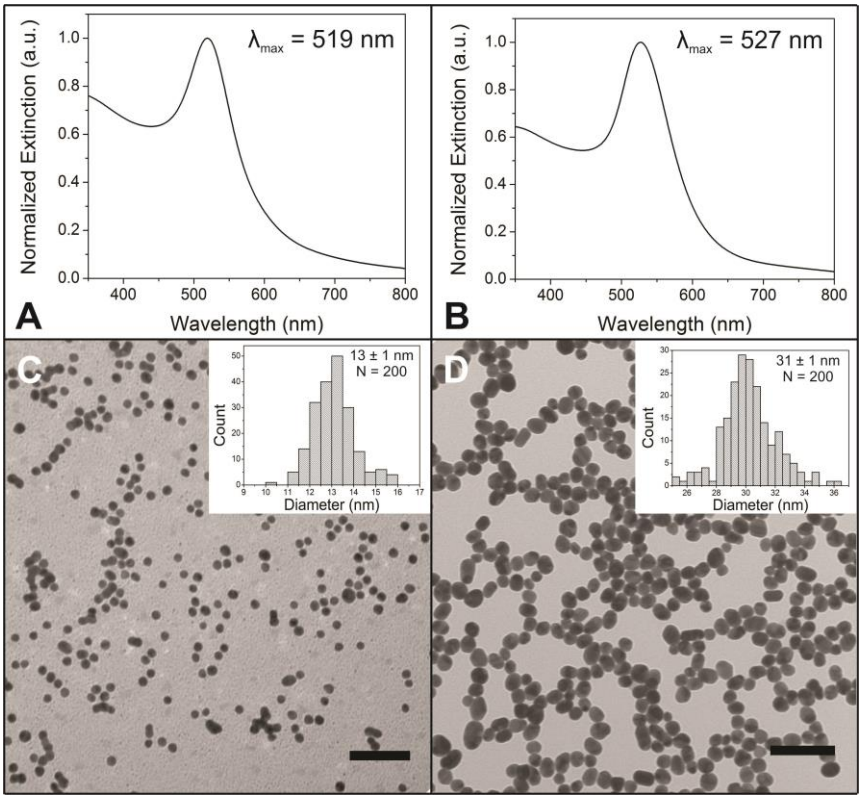


**Figure S1.** Representative UV-vis-NIR spectra for 13 nm (A) and 30 nm (B) NPs and corresponding TEM images, (C) and (D). Insets are histograms for 13 nm and 30 nm NPs generated from measurements of at least 200 NPs. Scale bars are 100 nm.

## UV-vis-NIR Analysis of AuNPs

Particles were characterized by ultraviolet-visible-near infrared (UV-vis-NIR) absorption spectroscopy using a Cary 5000 spectrophotometer (Agilent, Inc.). Spectra were baseline corrected with respect to the spectrum of water. In order to obtain each spectrum, the AuNP solution was diluted by 1/3 with NANOpure water.

## TEM Analysis of AuNPs for Size Determination

An aliquot from each final AuNP solution was diluted 1/5 with NANOpure water prior to drop casting onto a Formvar-coated copper transmission electron microscopy (TEM) grid (Ted Pella, Inc.). Samples were allowed to air dry and then dried under vacuum before characterization using an FEI Morgagni TEM at 80 kV. The size distributions of the AuNPs were determined from TEM images of at least 200 AuNPs from various areas of the grid. ImageJ 1.47d (National Institutes of Health, USA) was used to measure and count all particles.

**Complete Method for ICP-MS Analysis**

Inductively coupled plasma mass spectrometry (ICP-MS) analysis was performed using an argon flow with a NexION spectrometer (PerkinElmer, Inc.). An aqua regia solution was prepared with a 3:1 ratio of hydrochloric acid (Sigma-Aldrich, > 99.999% trace metal basis): nitric acid (Sigma-Aldrich, > 99.999% trace metal basis) and diluted with water for a 5% (by volume) aqua regia matrix. AuNP samples were taken from the concentrated pellet after ligand exchange as described in the Experimental Section and digested overnight in ~5 µL of fresh and concentrated aqua regia solution. From the digested solution, 1 µL was further diluted to 15 mL using 5% aqua regia matrix, and the remainder of the digest was reserved for $^{1}$H-NMR analysis (*vide infra*).

Unknown Au concentrations were determined by comparison to a 5-point standard curve with a range of 1 - 30 ppb (1, 5, 10, 20, and 30 ppb prepared by volume) from a gold standard for ICP (Fluka, TraceCERT 1,001 ± 2 mg/L Au in HCl) diluted in the 5% aqua regia matrix. All standards were measured 5 times and averaged, while all unknown samples were measured in triplicate and averaged. A 5 minute flush time with 5% aqua regia matrix was used between all runs, and a blank was analyzed before each unknown sample to confirm removal of all residual metals from the instrument.

**Table S1.** Conditions for synthesis of AuNPs with different diameters

| Molar Ratio (Au:Citrate) | Amount $HAuCl_4 \cdot 3H_2O$ (g) | Amount Trisodium Citrate (g) | Particle Size by TEM* (nm) |
|---|---|---|---|
| 1:3.31 | 0.1970 | 0.4857 | 13.01 ± 0.84 |
| 1:2.02 | 0.1971 | 0.2990 | 30.94 ± 1.13 |

*N ≥ 200 for all particle sizes, with average ± standard deviation.

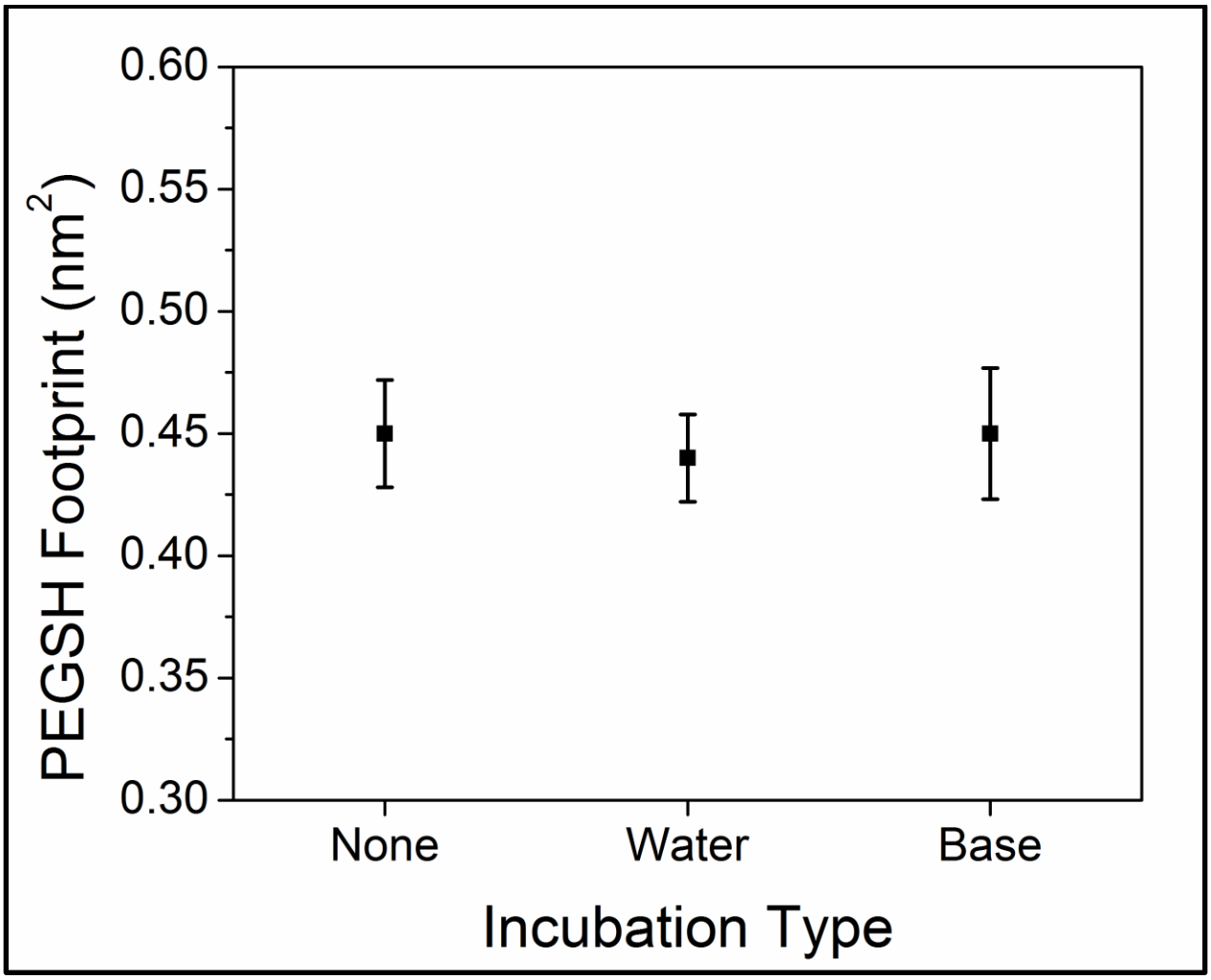


**Figure S2**. Comparison of PEGSH footprint measured from particles analyzed immediately after purification, analyzed after purification and subsequent incubation overnight in base (phosphate buffer, 10 mM, pH = 10), and analyzed after purification and subsequent incubation overnight in pure water, where error bars represent standard error of at least 5 trials. No significant difference is observed between the sets of AuNPs at a 95% confidence interval (*t* test).

**Minimum Ligand Footprint and Ligand Excess Determination:**

In order to form a full monolayer of surface adsorbed species, the concentration of ligand must be in some excess of available surface sites. Here, we estimate excess with respect to total available surface area of the AuNPs and the minimum theoretical footprint area of the incoming ligand on a flat gold surface. The total available surface area of the AuNPs is calculated from the concentration of AuNPs (determined by ICP-MS) and the average core diameter (determined by TEM) (Scheme S1). The minimum theoretical footprint of the incoming ligand was determined using a model system generated by the Avogadro molecular editor,[1] which was also used to aid in the measurement of atomic distances (Figure S3). Specifically, the geometry of an alkane thiol on a flat gold slab was geometrically optimized by relaxation with the universal force field (UFF) to an average force of $10^{-4}$ kJ/mol/atom before bond lengths and angles were obtained.

The length of carbon-hydrogen bonds were measured to be 1.112 Å and 1.111 Å for each carbon-hydrogen bond, with the slight (0.001 Å) variation observed depending on the presence of adjacent molecules (Figure S3). This measurement is from one atom center to the other. Therefore, the van der Waals sphere must also be considered, where the van der Waals radius for hydrogen was estimated to be 1.09 Å.[2] The linear distance between carbon atoms in the alkane chain was calculated to be 0.509 Å by considering the triangular geometry indicated below. By summing the bond lengths (Figure S3B), we obtain an overall molecular diameter estimate of 0.491 nm and corresponding minimum footprint of 0.189 $nm^2$/ligand. From this footprint, a maximum of 2,813 ligands could be added to the surface of a 13 nm AuNP. This minimum footprint value is used only to estimate percent excess incoming ligand with respect to AuNP surface area.

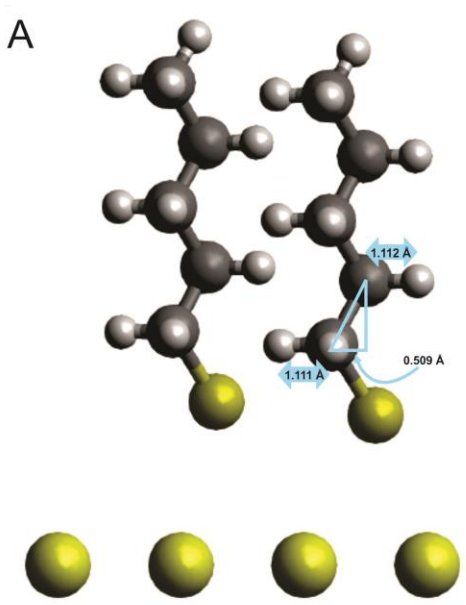


B

1.111 Å (for C-H bond)
1.112 Å (for C-H bond)
0.509 Å (for distance between C-C)
+ 2(1.09 Å) (for each van der Waals radius of H)
4.912 Å (total estimated diameter of ligand)

**Figure S3.** Representative molecule for minimum ligand occupation area of alkane thiol ligands on a flat gold surface (A) and corresponding calculation for ligand "diameter" based on the estimated geometry (B).

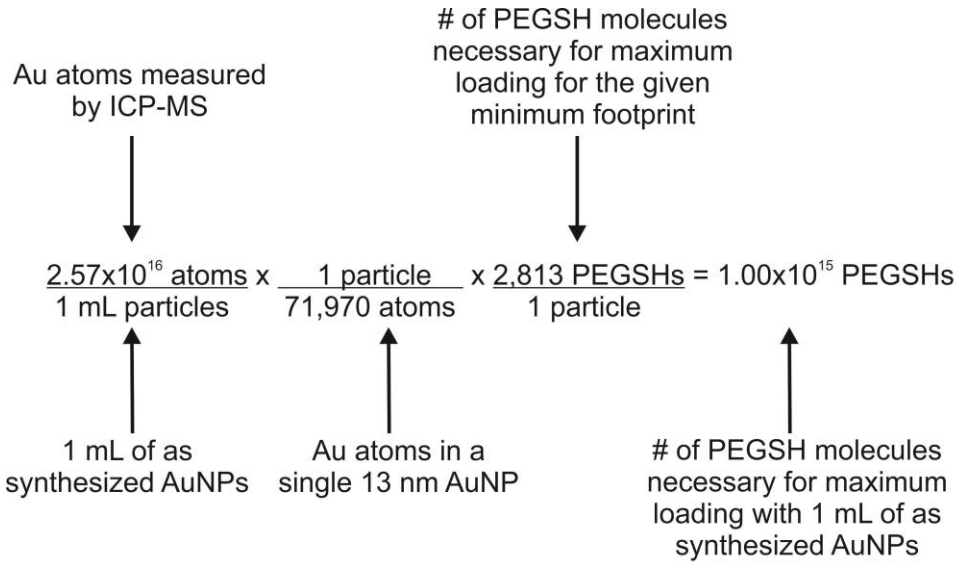


**Scheme S1**. Sample calculation for determining the number of PEGSH molecules necessary to achieve complete AuNP coverage with a 0x excess on 1 mL of 13 nm AuNPs, as synthesized.

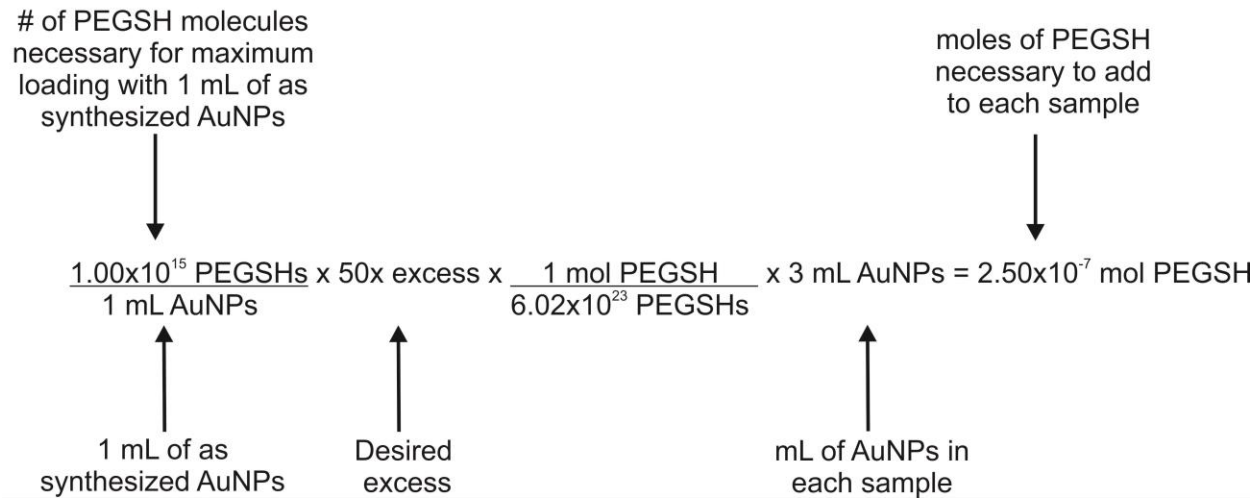


**Scheme S2**. Sample calculation for determining the number of moles of PEGSH necessary for a 50x excess of PEGSH with respect to NP surface area.

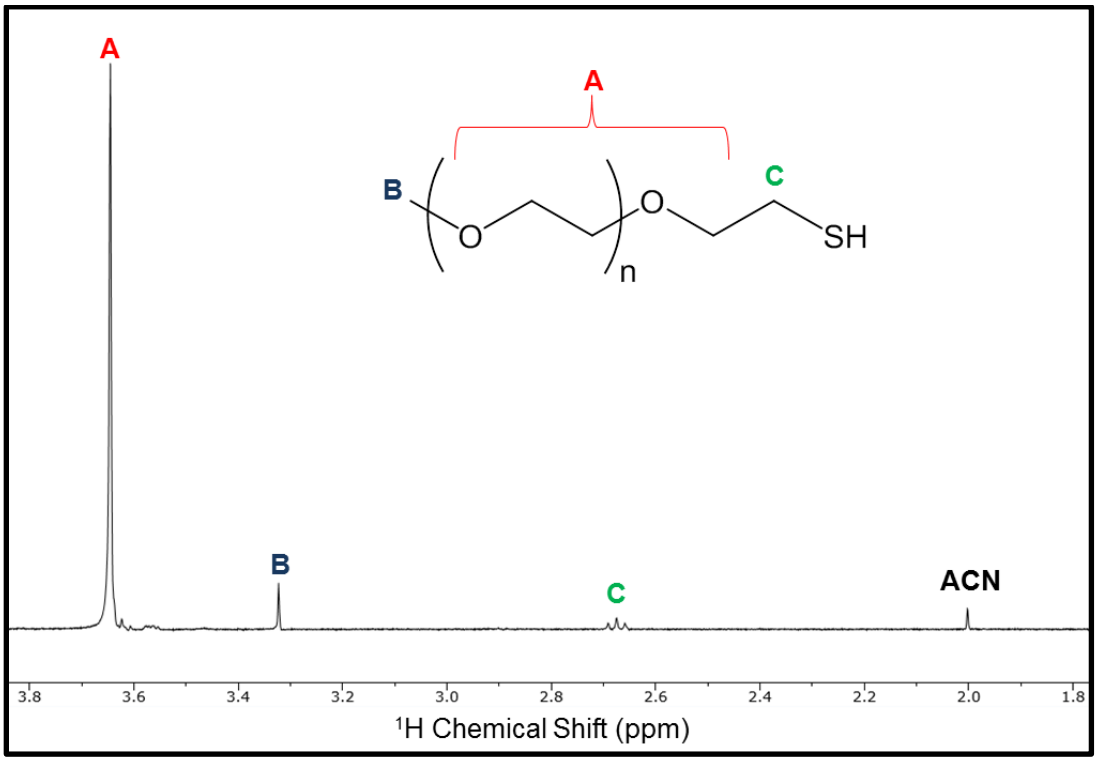


**Figure S4**. Representative $^{1}$H NMR spectrum of PEGSH in $D_2O$ with its labeled structure corresponding to plotted $^{1}$H NMR peak locations. For calculation of PEGSH concentration, Peak A is integrated and compared to the integrated intensity of the ACN peak.

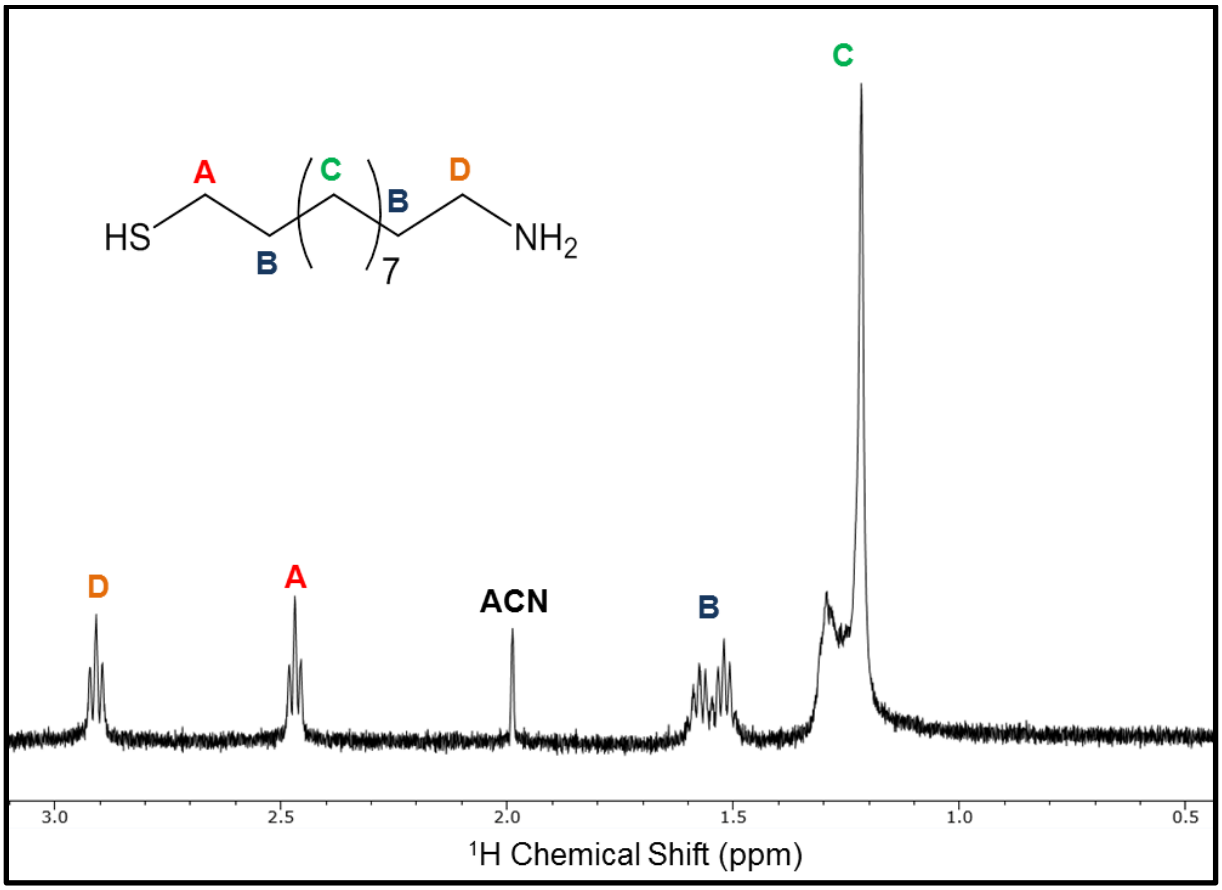


**Figure S5**. Representative $^{1}$H NMR spectrum of AUT in $D_2O$ with its labeled structure corresponding to plotted $^{1}$H NMR peak locations. For calculation of AUT concentration, Peak C is integrated and compared to the integrated intensity of the ACN peak. Peaks from both the thiol and amine protons are not observed, as they exchange with the surrounding deuterated medium.

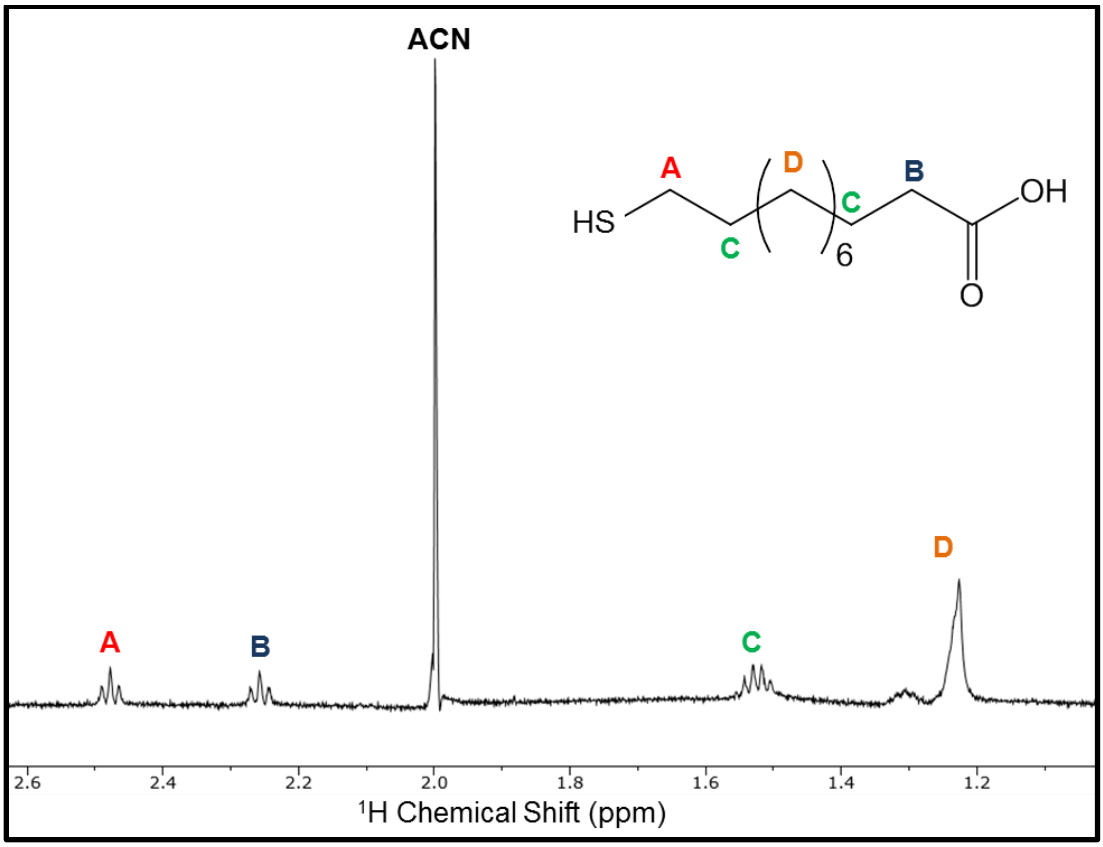


**Figure S6**. Representative $^{1}H$ NMR spectrum of MUA in $D_2O$ with its labeled structure corresponding to plotted $^{1}H$ NMR peak locations. For calculation of MUA concentration, Peak D is integrated and compared to the integrated intensity of the ACN peak.

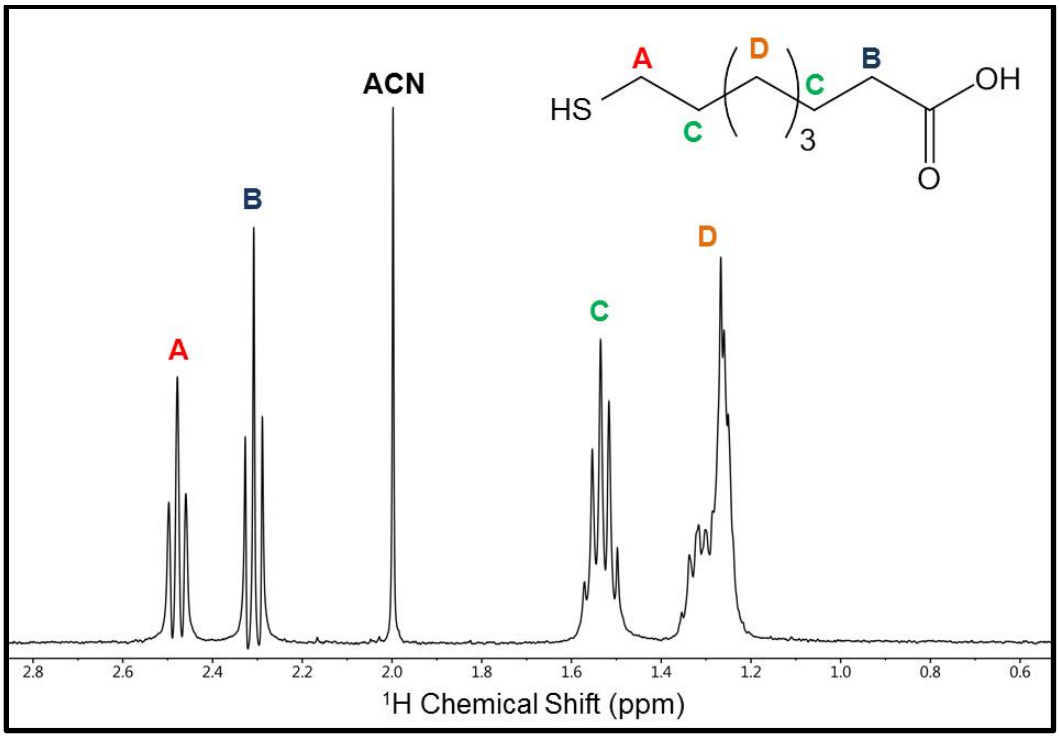


**Figure S7**. Representative $^{1}$H NMR spectrum of MOA in $D_2O$ with its labeled structure corresponding to plotted $^{1}$H NMR peak locations. For calculation of MOA concentration, Peak D is integrated and compared to the integrated intensity of the ACN peak.

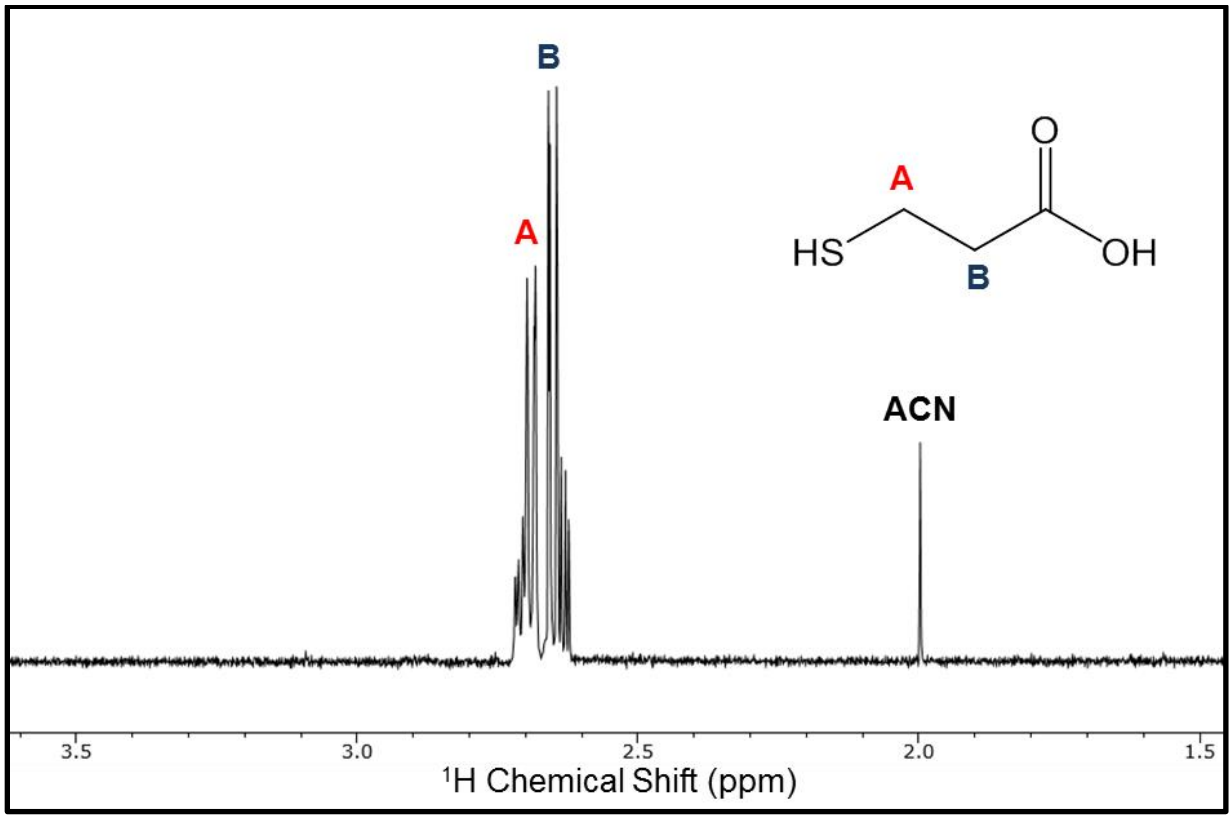


**Figure S8**. Representative $^{1}H$ NMR spectrum of MPA in $D_2O$ with its labeled structure corresponding to plotted $^{1}H$ NMR peak locations. For calculation of MPA concentration, Peaks A and B (due to peak overlap) are integrated and compared to the integrated intensity of the ACN peak.

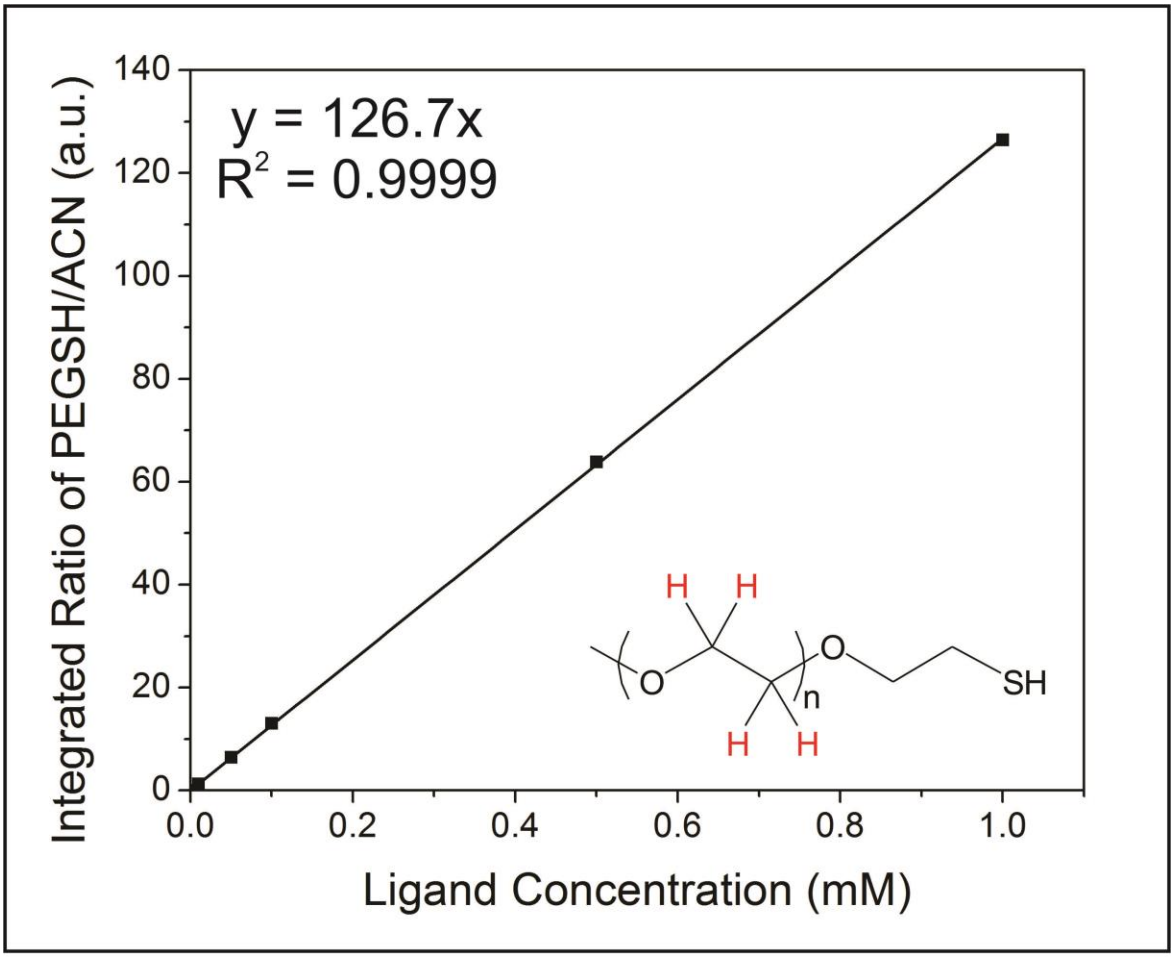


**Figure S9**. Sample calibration curve obtained for PEGSH by plotting integrated ratios of PEGSH/ACN against the concentration of PEGSH. PEGSH protons used for this analysis are highlighted in red.

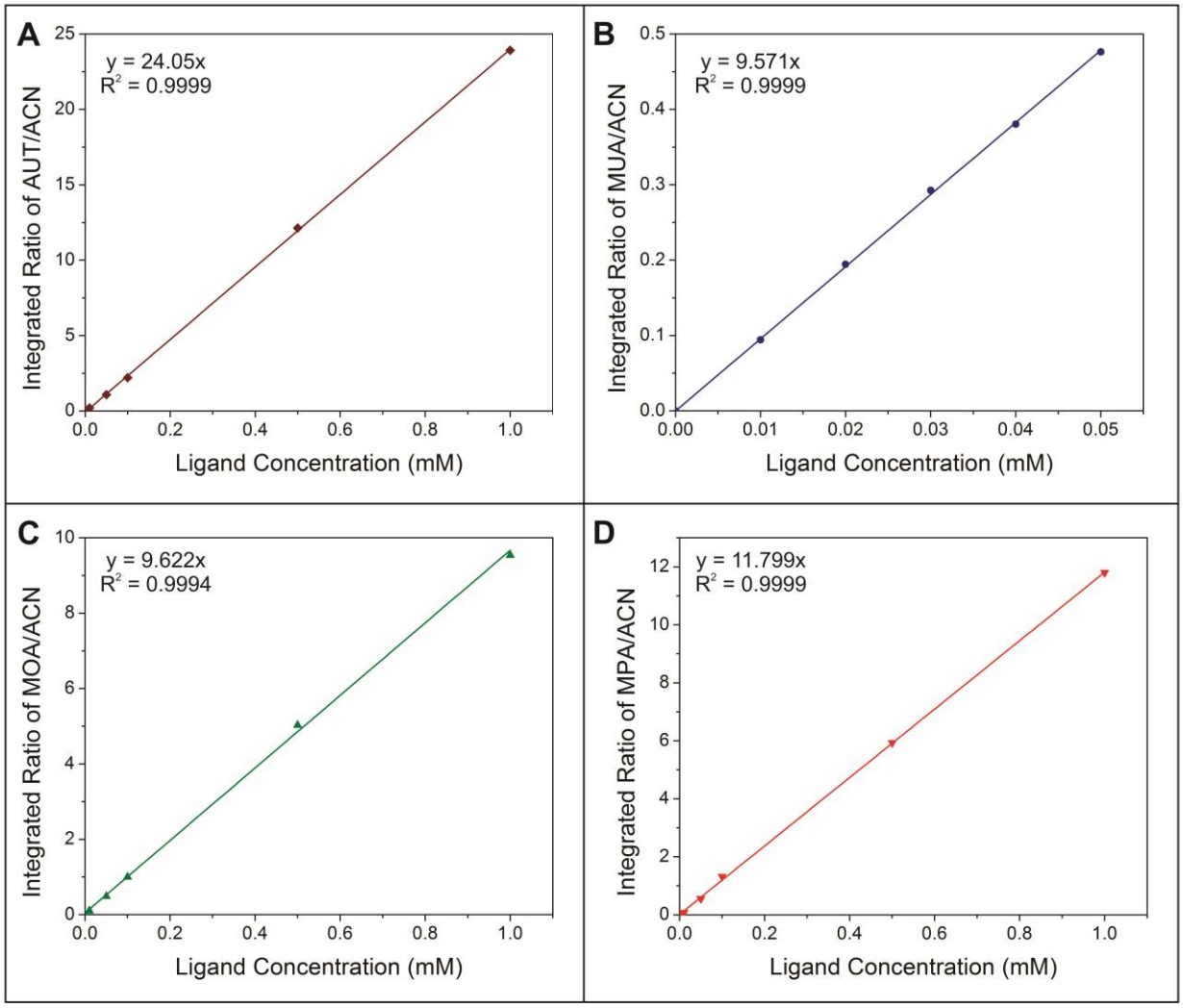


**Figure S10**. Representative calibration curves obtained for AUT (A), MUA (B), MOA (C), and MPA (D) by plotting integrated ratios of specific protons from each respective ligand (see Figures S5 – S8)/ACN against the concentration of that ligand to yield the equation for the line that will generate the unknown concentrations for each ligand.

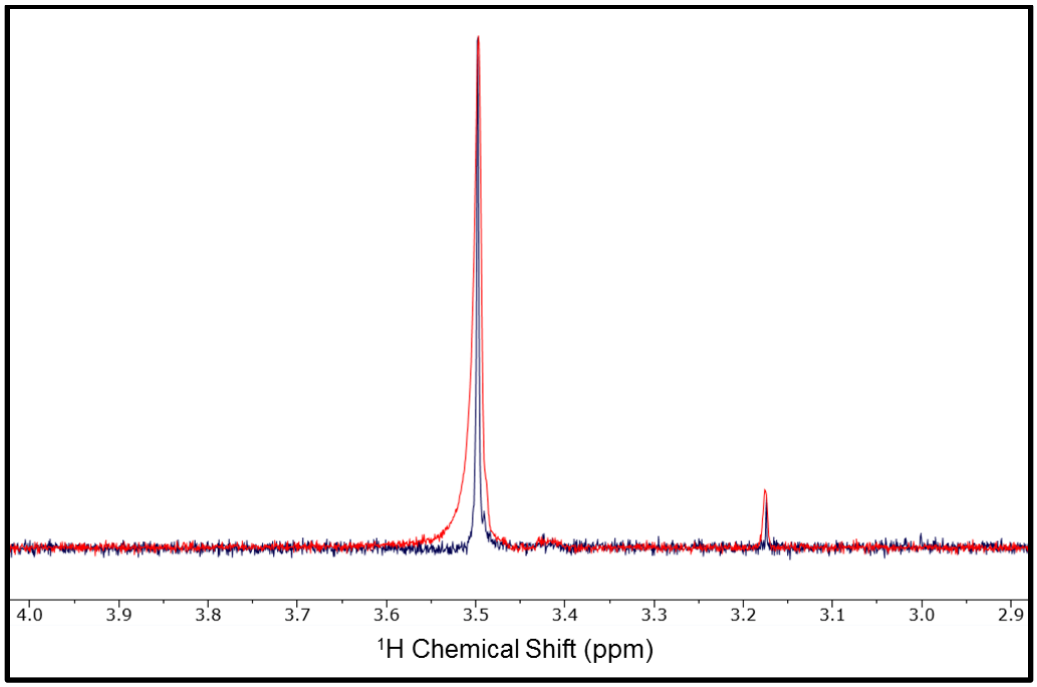


**Figure S11.** Representative $^{1}$H NMR spectra of PEGSH on-particle (red line) and off-particle (blue line) in $D_2O$ for 13 nm AuNPs. Line broadening observed with the on-particle spectrum can obscure accurate quantification. *N. B.* see main text for physical explanation.

**Synthetic and Characterization Details for PEGSeCN**

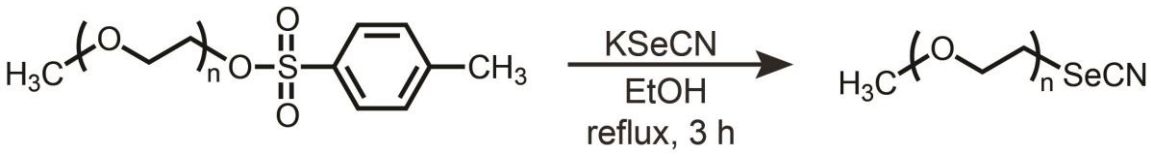


Poly(ethylene glycol) methyl ether tosylate (PEG-tosylate, average $M_n$ = 900, $Đ$ < 1.1) and potassium selenocyanate (KSeCN) were purchased from Sigma-Aldrich and used as received. KSeCN (60 mg, 0.416 mmol) was dissolved in anhydrous ethanol (0.22 mL) and heated to 80°C in a 3-neck round bottom flask with a reflux condenser under an argon atmosphere. PEG-tosylate (333 mg) was added dropwise and an additional 0.2 mL of anhydrous ethanol was used to rinse the storage vessel. The mixture was stirred for 3 hours under reflux with an additional 1.2 mL of ethanol being added periodically over the course of the reaction to maintain constant volume and ensure dissolution of the salts. The mixture was then cooled to room temperature and the solvent removed by rotary evaporation. The crude product was then dissolved in ether (5 mL) and washed with 0.1 M NaOH (3 x 5 mL) and brine (3 x 5 mL). The aqueous fraction was concentrated, and the resultant solid stirred with ether (50 mL) for 20 minutes and filtered. This was repeated 3 times, and the combined ether washes

were concentrated to give the product as a pale yellow semi-solid (124 mg). $^{1}$H NMR (400 MHz, $D_2O$) δ 3.62 (s, 64H), 3.30 (s, 3H), 3.09 (t, 3H).

Mass spectrum was obtained using a JEOL AccuTOF model JMS-T1000LC mass spectrometer equipped with a Direct Analysis in Real Time (DART) ion source in the positive ion mode.

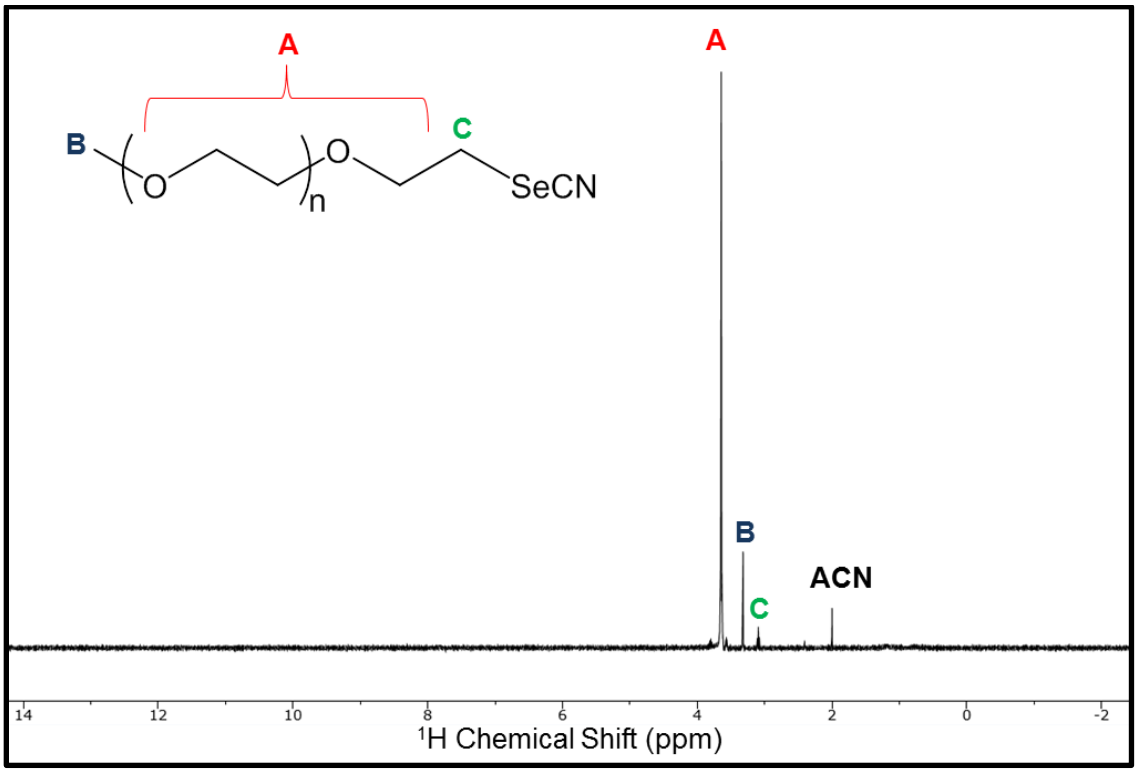


**Figure S12**. Representative $^{1}$H NMR spectrum of PEGSeCN acquired in $D_2O$.

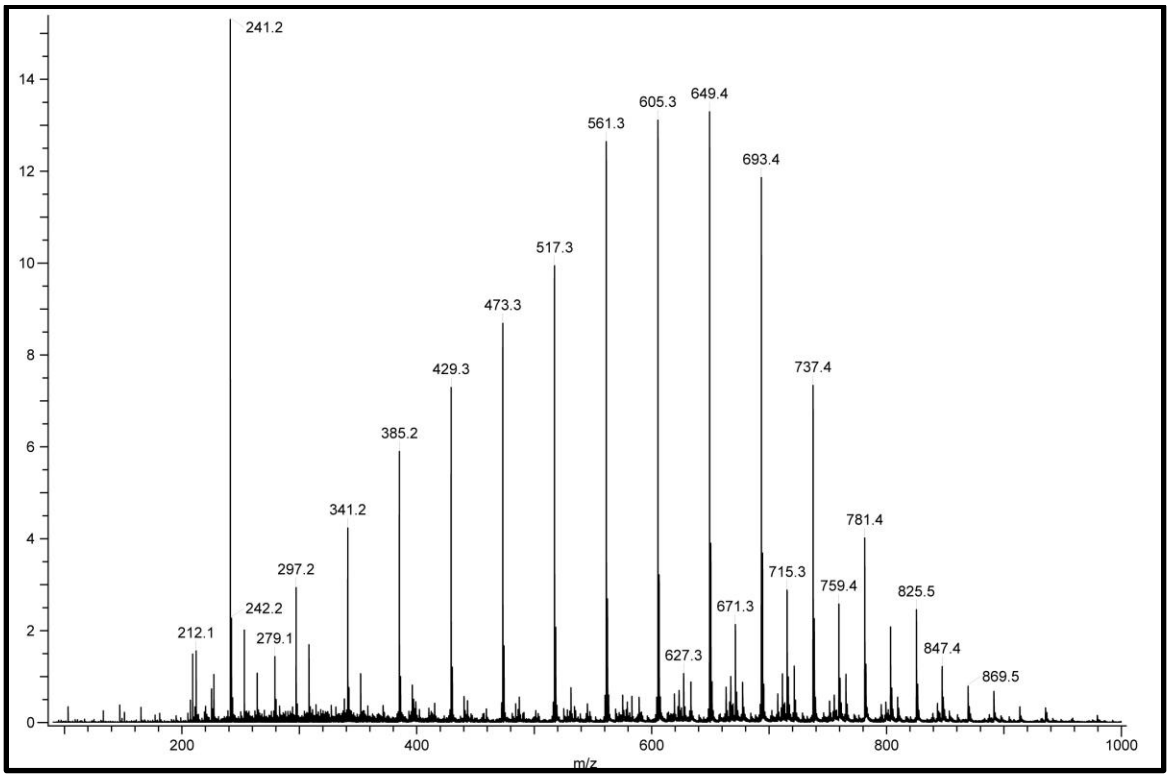


**Figure S13**. Representative mass spectrum (DART ionization, positive ion mode) of PEGSeCN.

Ligand exchange with the PEGSeCN was performed similarly to the procedure for the citrate to PEGSH exchange described in the Experimental Section. Prior to use, the AuNPs were filtered using 25 mm GD/XP disposable filters with PVDF filter membrane with a pore size of 0.45 µm (Whatman, Inc.) to remove any large particulates. Immediately after filtration, the AuNPs were concentrated by separating 1 mL aliquots into 1.5 mL centrifuge tubes and centrifuging the reaction mixture at 20,000 rcf for 5 minutes (Eppendorf 5424 centrifuge). The supernatant was removed, and another 1 mL aliquot of filtered particles was added. The pellet was resuspended, and the process was repeated until 3 mL of filtered particles were concentrated to 1 mL in centrifuge tubes. The particles were centrifuged once more, and the supernatant was removed. The pellet was resuspended in 50 µL of 5 mM PEGSeCN and 950 µL of water. This mixture was then placed on a temperature controlled mixer for 48 hours at 1,000 rpm and 25 °C. After these 48 hours, the particles were washed twice. After the washing cycles, the particles were resuspended in a mixture of 990 µL of water and 10 µL of 100 mM pH 10 phosphate buffer. This mixture was placed on a temperature controlled mixer overnight at 1,000 rpm and 25 °C. After this time, the particles were washed with phosphate buffer twice, followed by 2 washes in water and 2 washes in $D_2O$. After the last wash cycle, the supernatant was removed to yield a concentrated pellet of PEGSeCN-capped AuNPs.

## ICP-OES Analysis of PEGSeCN

ICP-OES analysis was performed using an argon flow with an Optima spectrometer (Perkin Elmer, Inc.). An aqua regia solution was prepared with a 3:1 ratio of hydrochloric acid (Sigma Aldrich, > 99.999% trace metal basis): nitric acid (Sigma Aldrich, > 99.999% trace metal basis) and diluted with water for a 5% v/v aqua regia matrix. AuNP samples capped with the PEGSeCN ligand were taken from the concentrated pellet after ligand exchange as described above and digested overnight in ~5 µL of fresh and concentrated aqua regia solution. The digested solution was diluted to a volume of 500 µL in $D_2O$ for $^1H$ NMR analysis. After analysis by NMR, 400 µL was further diluted to 2.5 mL using the 5% aqua regia matrix. Unknown Se concentrations were determined by comparison to a 5-point standard curve with a range of 0.10 - 10 ppm (0.10, 0.50, 1.0, 5.0, and 10 ppm prepared by volume), from a selenium standard for ICP (Fluka, TraceCERT 1000 ± 2 mg/L Se in $HNO_3$) diluted in 5% aqua regia matrix. All standards were measured 5 times and averaged, while all unknown samples were measured in triplicate and averaged. A 7 minute flush time with 5% aqua regia matrix was used between all runs, and a blank was analyzed before each unknown sample to confirm removal of all residual metals from the instrument.

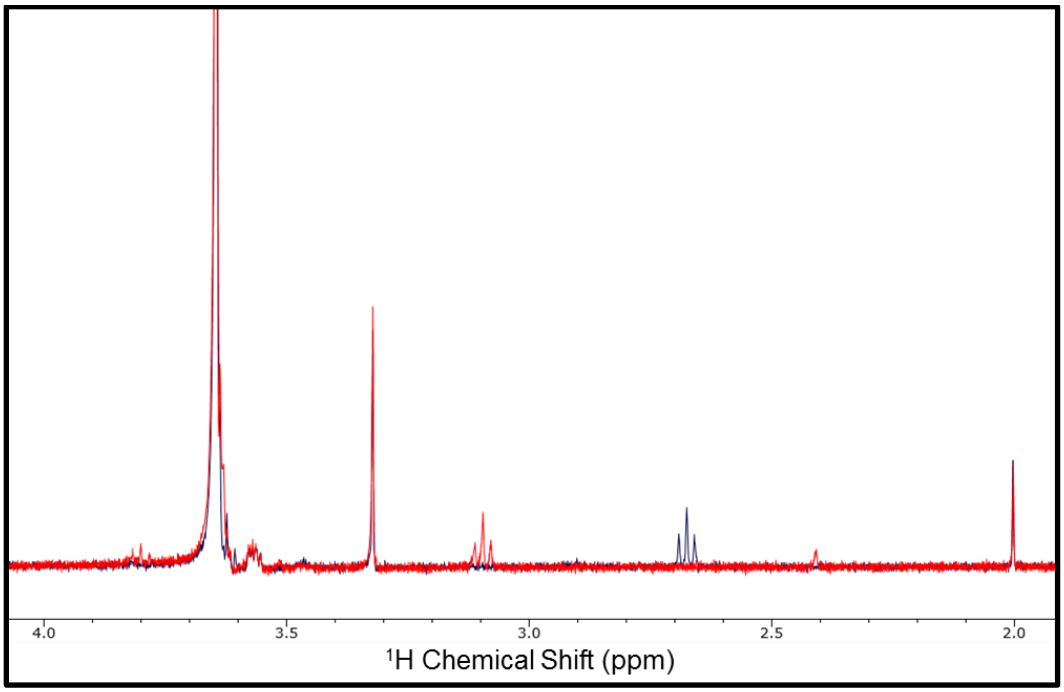


**Figure S14**. Representative $^1H$ NMR spectra of PEGSeCN (red) and PEGSH (blue). The discrepancy in the peak at 3.1 ppm (for the PEGSH) and 2.68 ppm (for the PEGSeCN) is due to the location of the protons on the carbon adjacent to either the sulfur (in PEGSH) or the selenium (in PEGSeCN).

**Analytical Comparison of NMR and ICP-OES**

A paired *t* test was used to compare the NMR and ICP-OES ligand quantification results according to the following equation:

$$t_{calculated} = \frac{|\bar{d}|}{s_d}\sqrt{n}$$

where $s_d$ is the standard deviation for each of the differences between the two measurements obtained with each method, $\bar{d}$ is the absolute value of the average difference between the two measurements obtained with each method, and n represents the number of trials.[3] A value of 2.11 is obtained for $t_{calculated}$. Comparing to $t_{table}$, which is equal to 2.262 for the 95% confidence interval, $t_{calculated}$ is less than $t_{table}$, indicating that the results obtained using the two methods are not statistically different.

Additionally, an F test was used to compare the standard deviations of the methods according to the following equation:

$$F_{calculated} = \frac{s_1^2}{s_2^2}$$

where $s_1$ and $s_2$ are the standard deviations for each method;[3] in this case, both are equal to 0.04. With these standard deviations, a value of 1.00 is obtained for $F_{calculated}$. Comparing to $F_{table}$, which gives a value of 3.18 at the 95% confidence interval for 10 trials of each method, $F_{calculated}$ is less than $F_{table}$ indicating that the difference between the standard deviations is not statistically significant.

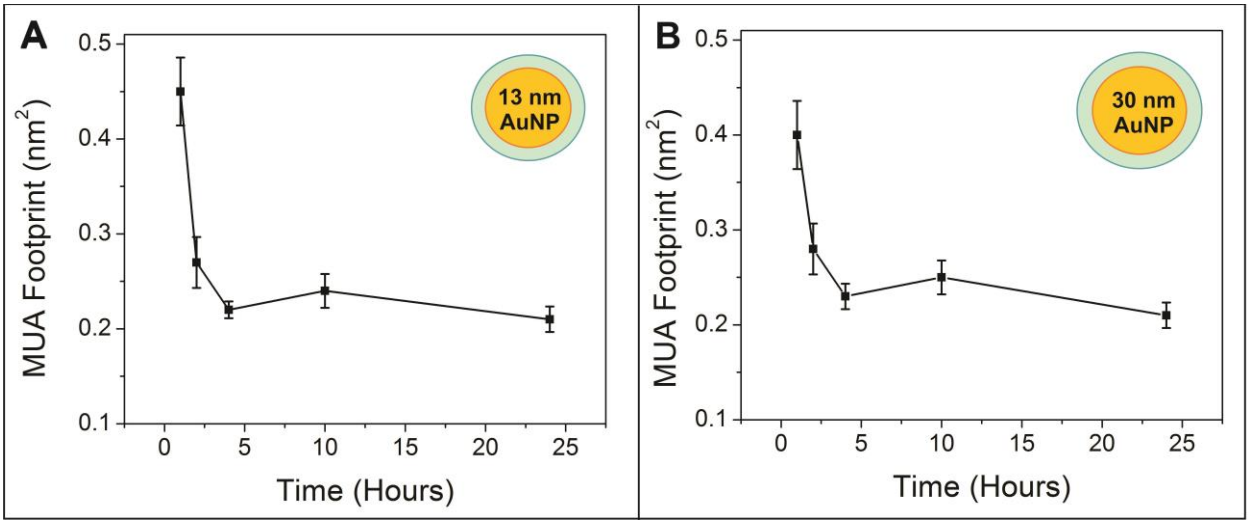


**Figure S15**. Plots of MUA footprint on the nanoparticle surface as a function of AuNP time in excess MUA (50x) for 13 nm (A) and 30 nm (B) AuNPs, where error bars represent the standard error of at least 5 trials. Results indicate that ligand loading reaches a plateau on the timescale of 2-3 hours under the conditions tested.

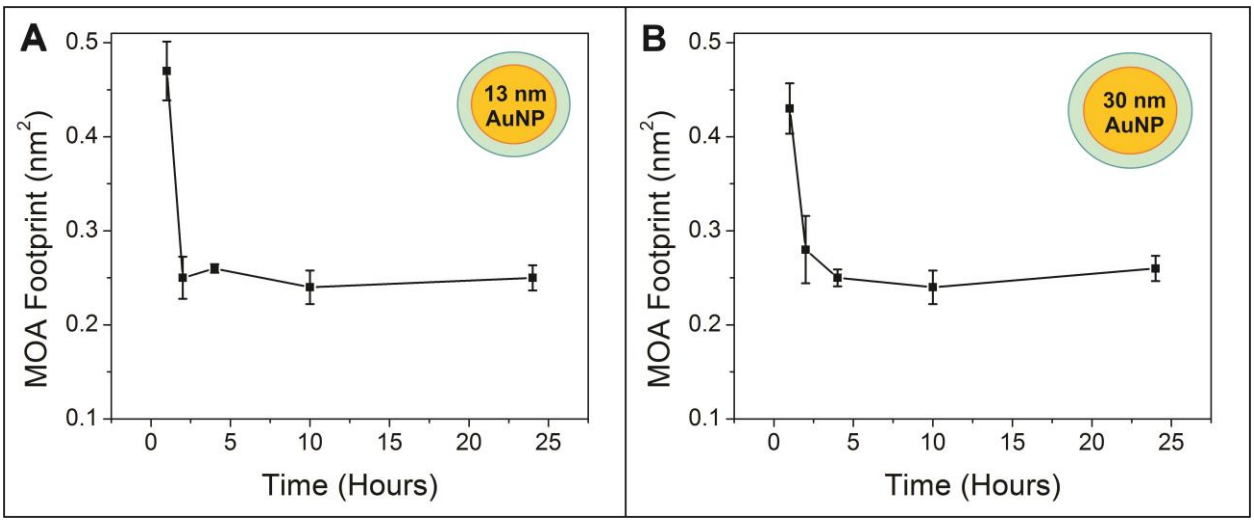


**Figure S16**. Plots of MOA footprint on the nanoparticle surface as a function of AuNP time in excess MOA (50x) for 13 nm (A) and 30 nm (B) AuNPs, where error bars represent the standard error of at least 5 trials. Results indicate that ligand loading reaches a plateau on the timescale of 2-3 hours under the conditions tested.

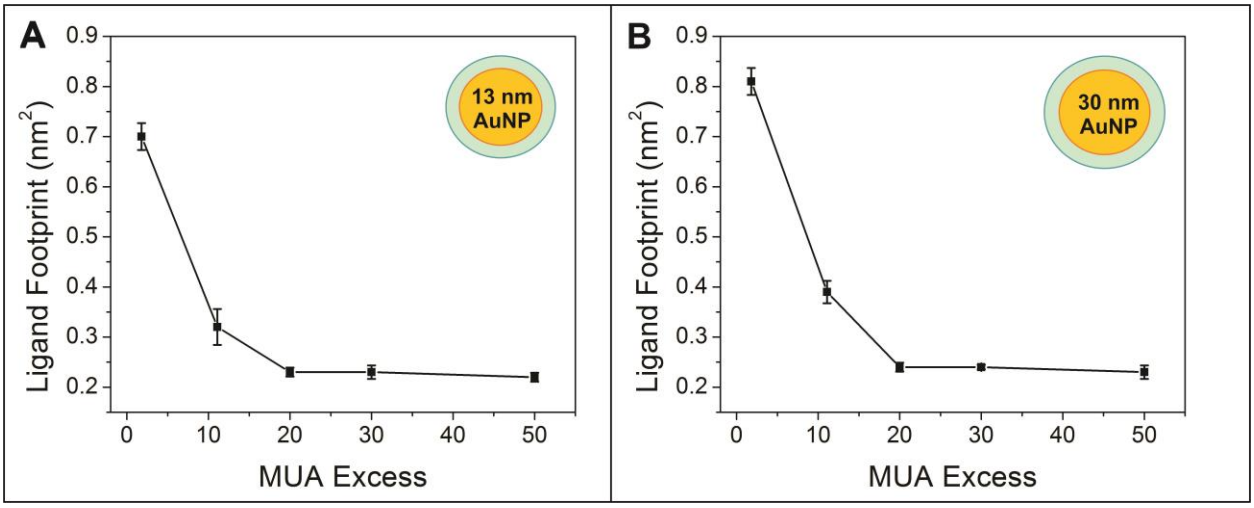


**Figure S17**. Graphs displaying MUA ligand footprint as a function of MUA excess with respect to surface area after 4 hours for 13 nm (A) and 30 nm (B) AuNPs, where error bars represent the standard error of at least 5 trials. Results indicate that loading reaches a consistent value at a ligand excess above 20x.

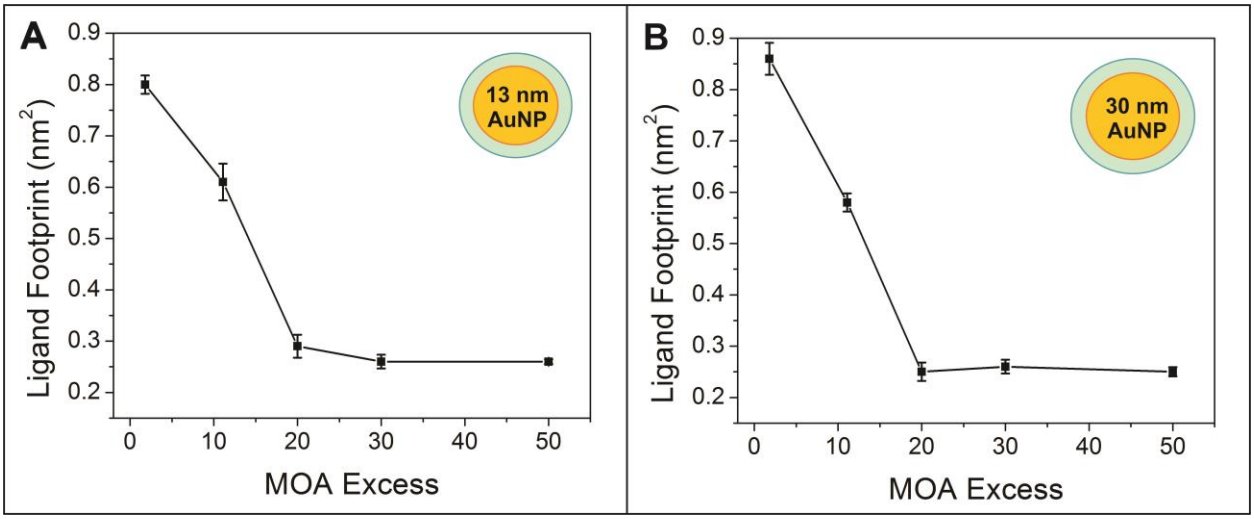


**Figure S18**. Graphs displaying MOA ligand footprint as a function of MOA excess with respect to surface area after 4 hours for 13 nm (A) and 30 nm (B) AuNPs, where error bars represent the standard error of at least 5 trials. Results indicate that loading reaches a consistent value at an excess above 20x.

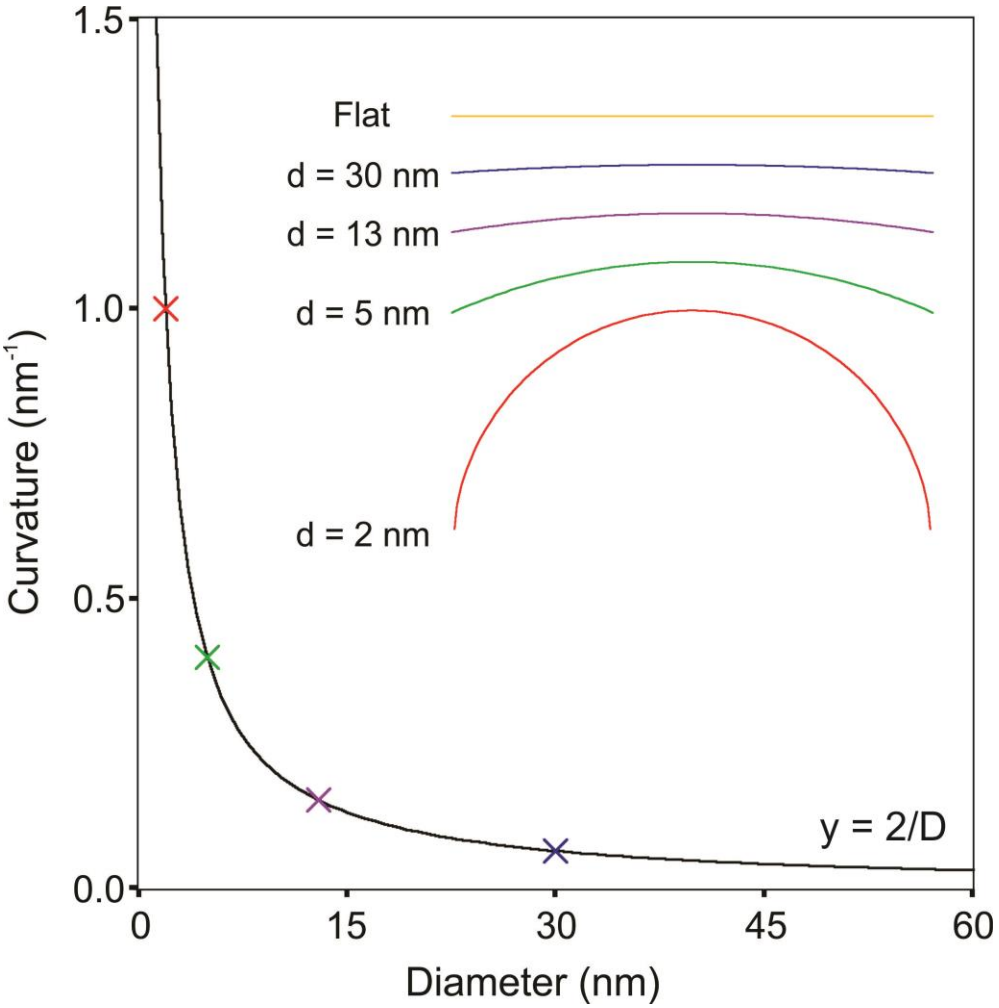


**Figure S19**. Surface curvature as a function of particle diameter. The figure illustrates that for particles with diameters larger than 10 nm, change in curvature as a function of particle diameter decreases dramatically.

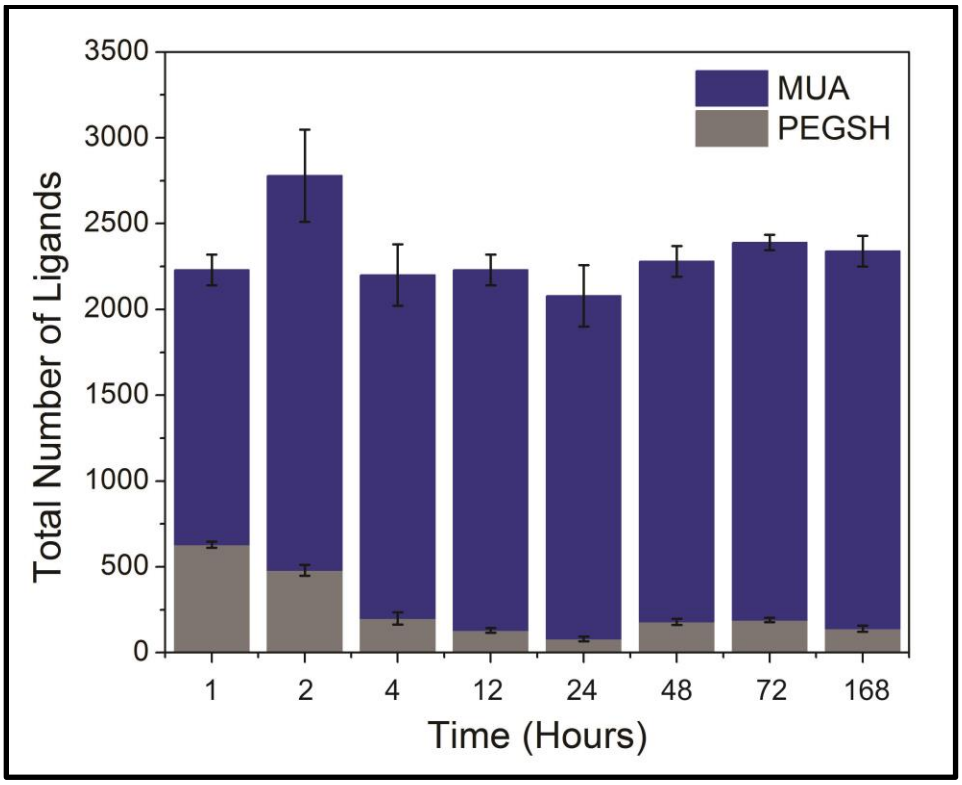


**Figure S20.** Graph of the total number of ligands on PEGSH AuNPs backfilled with MUA as a function of time for 13 nm AuNPs, where the error bars represent the standard error of at least 5 trials. Results indicate that ligand loading reaches consistent values on the timescale of 2-3 hours under the conditions tested.

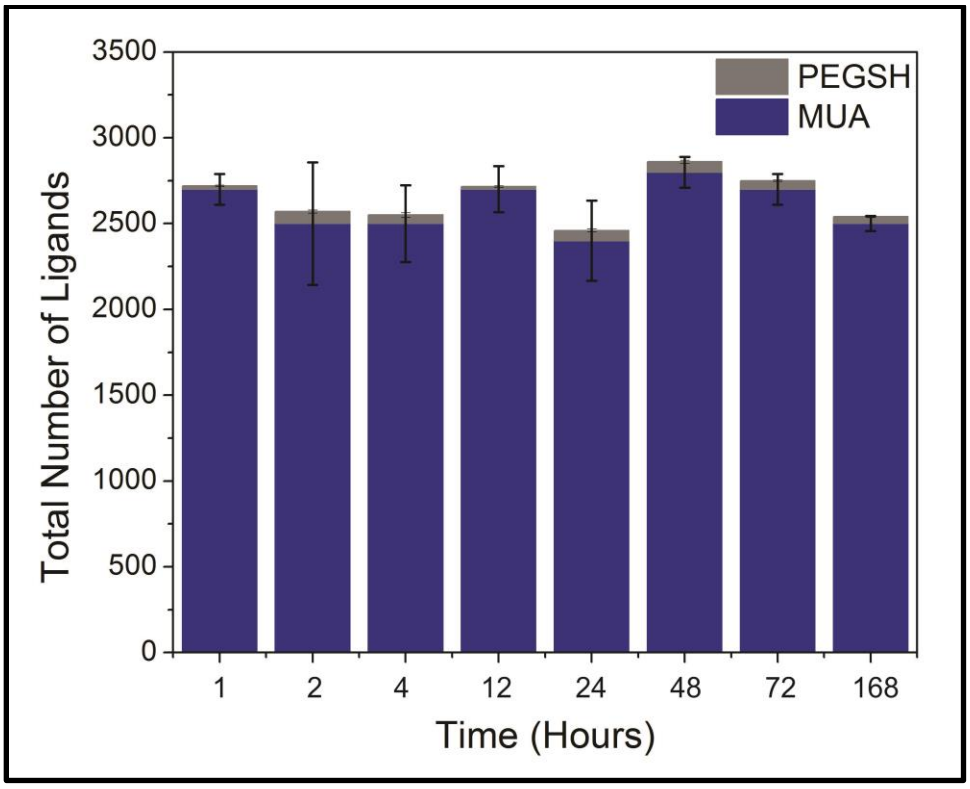


**Figure S21.** Graph of the total number of ligands on MUA AuNPs backfilled with PEGSH as a function of time for 13 nm AuNPs, where the error bars represent the standard error of at least 5 trials. Results indicate that ligand loading reaches consistent values on the timescale of 2-3 hours under the conditions tested.

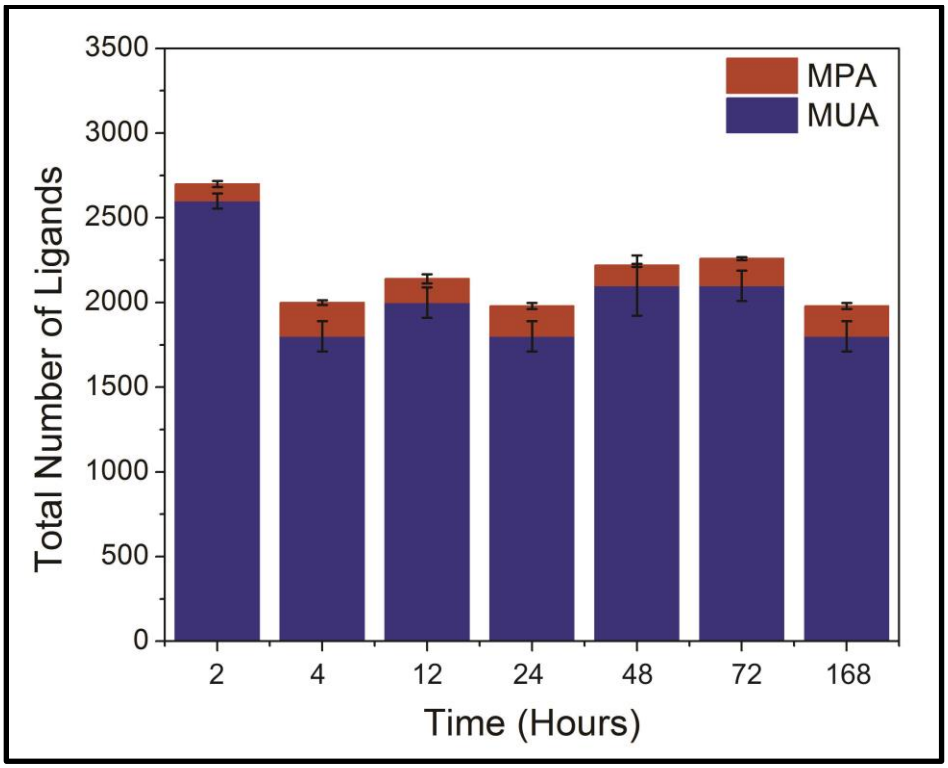


**Figure S22.** Graphs of the total number of ligands on MUA AuNPs backfilled with MPA as a function of time for 13 nm AuNPs, where the error bars represent the standard error of at least 5 trials. Results indicate that ligand loading reaches consistent values on the timescale of 2-3 hours under the conditions tested.

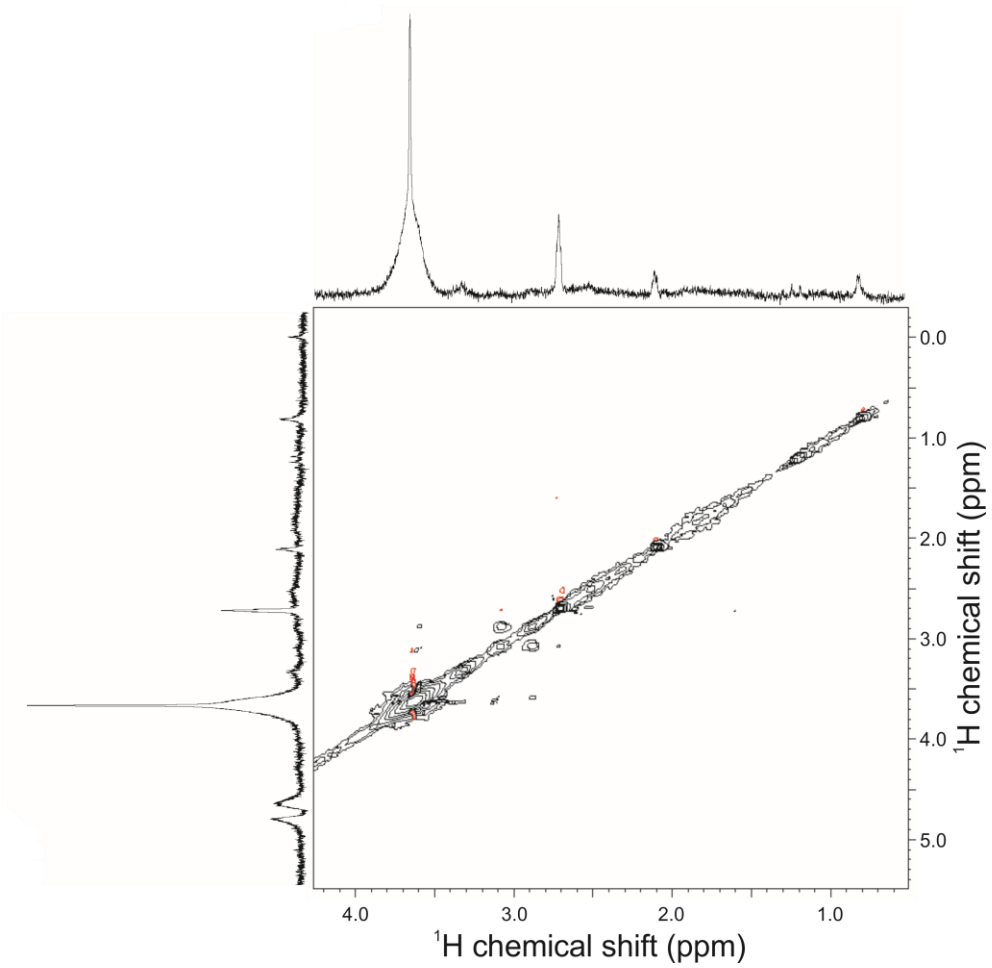


**Figure S23**. $^1$H-$^1$H Nuclear Overhauser Effect Spectroscopy (NOESY) of 13 nm AuNPs capped with PEGSH and ligand exchanged with MUA acquired with a 400 ms mixing time. MUA does not show any cross peaks with the PEGSH ligand, consistent with a segregated ligand shell architecture consisting of MUA and PEGSH domains. The formation of thiolated, small-molecule islands that are segregated from the original PEGSH shell are consistent with a cooperative binding mechanism for ligand exchange. The peaks at 4.7 ppm in the indirect dimension result from incomplete water suppression. The positive artifacts (red) on the PEGSH diagonal are residual $T_1$ noise that could not be completely removed.

**Particle size and size distribution after ligand exchanges**

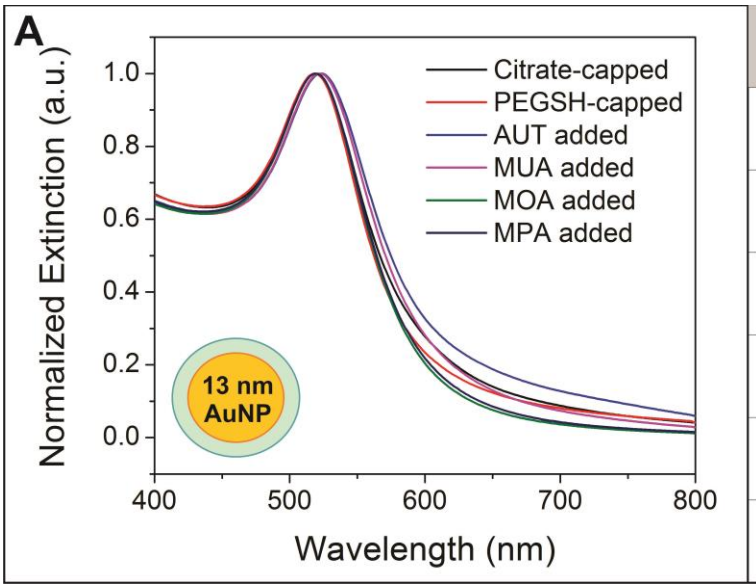


| B | $\lambda_{max}$ (nm) | Size (nm) |
|---|---|---|
| Citrate-capped | 519 | 13 ± 1 |
| PEGSH-capped | 518 | 13 ± 1 |
| AUT added | 523 | 14 ± 1 |
| MUA added | 522 | 13 ± 1 |
| MOA added | 520 | 13 ± 1 |
| MPA added | 520 | 13 ± 1 |

**Figure S24**. UV-vis spectra for all 13 nm PEGSH-functionalized AuNPs before and after secondary ligand addition (A). No significant change in particle size is observed (average ± standard deviation) (B).

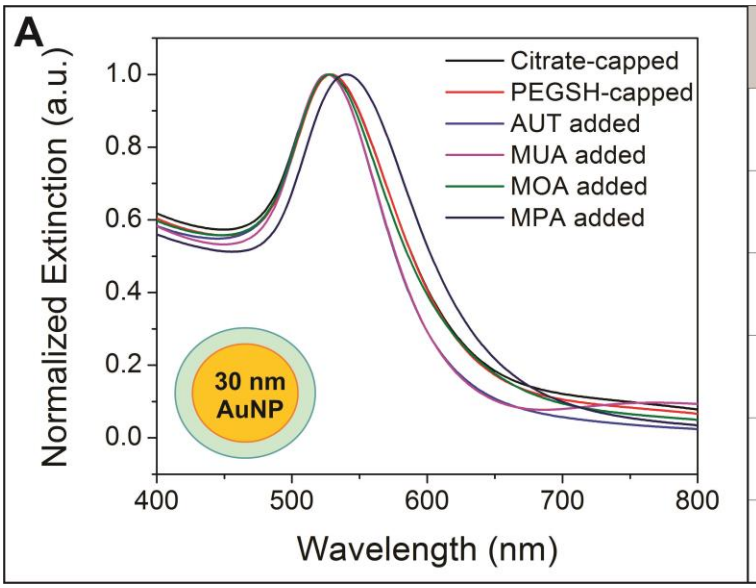


| B | $\lambda_{max}$ (nm) | Size (nm) |
|---|---|---|
| Citrate-capped | 529 | 31 ± 1 |
| PEGSH-capped | 530 | 31 ± 1 |
| AUT added | 528 | 32 ± 2 |
| MUA added | 531 | 31 ± 1 |
| MOA added | 530 | 31 ± 1 |
| MPA added | 540 | 32 ± 1 |

**Figure S25**. UV-vis spectra for all 30 nm PEGSH-functionalized AuNPs before and after secondary ligand addition (A). No significant change in particle size is observed (average ± standard deviation) (B).

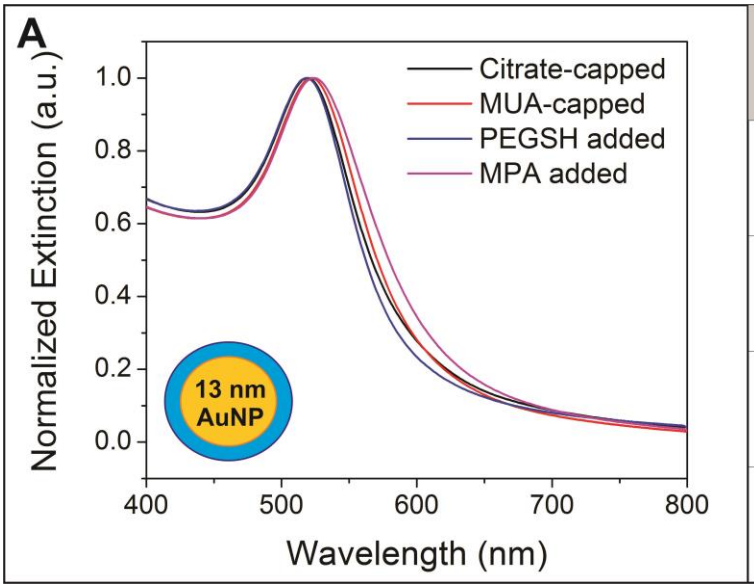


| B | $\lambda_{max}$ (nm) | Size (nm) |
|---|---|---|
| Citrate-capped | 519 | 13 ± 1 |
| MUA-capped | 522 | 13 ± 1 |
| PEGSH added | 518 | 14 ± 1 |
| MPA added | 524 | 14 ± 1 |

**Figure S26**. UV-vis spectra for all 13 nm MUA-functionalized AuNPs before and after secondary ligand addition (A). No significant change in particle size is observed (average ± standard deviation) (B).

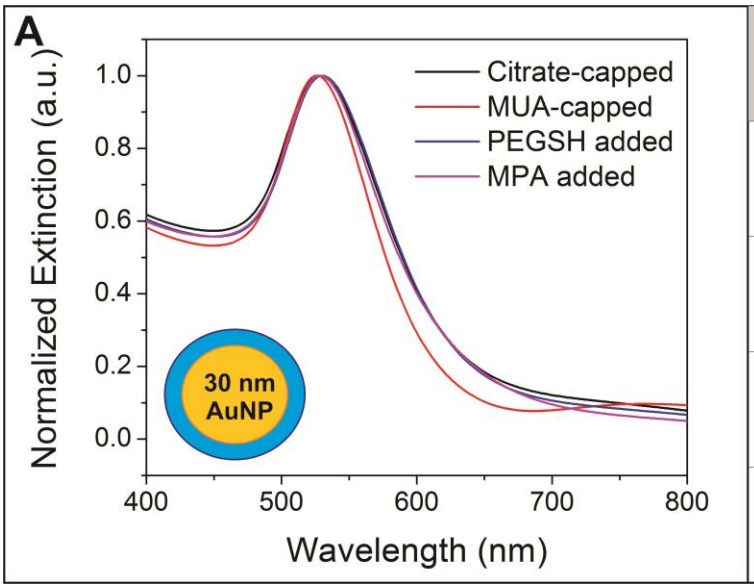


| B | $\lambda_{max}$ (nm) | Size (nm) |
|---|---|---|
| Citrate-capped | 529 | 31 ± 1 |
| MUA-capped | 531 | 32 ± 1 |
| PEGSH added | 530 | 32 ± 1 |
| MPA added | 532 | 32 ± 2 |

**Figure S27**. UV-vis spectra for all 30 nm MUA-functionalized AuNPs before and after secondary ligand addition (A). No significant change in particle size is observed (average ± standard deviation) (B).

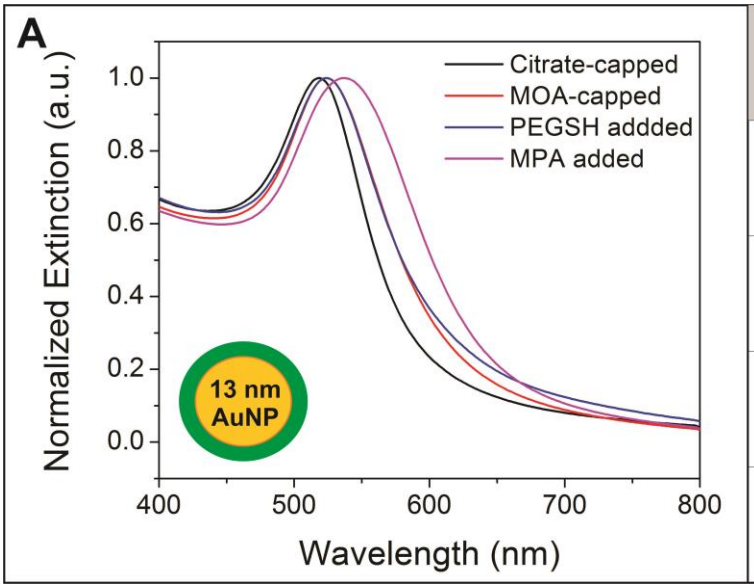


| B | $\lambda_{max}$ (nm) | Size (nm) |
|---|---|---|
| Citrate-capped | 519 | 13 ± 1 |
| MOA-capped | 520 | 13 ± 1 |
| PEGSH added | 520 | 14 ± 1 |
| MPA added | 536 | 14 ± 1 |

**Figure S28**. UV-vis spectra for all 13 nm MOA-functionalized AuNPs before and after secondary ligand addition (A). No significant change in particle size is observed (average ± standard deviation) (B).

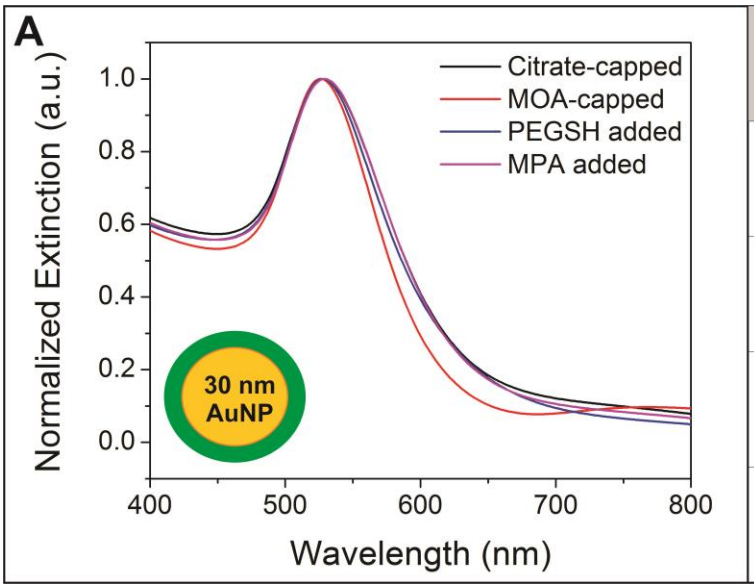


| B | $\lambda_{max}$ (nm) | Size (nm) |
|---|---|---|
| Citrate-capped | 529 | 31 ± 1 |
| MOA-capped | 530 | 31 ± 1 |
| PEGSH added | 528 | 32 ± 1 |
| MPA added | 531 | 32 ± 1 |

**Figure S29**. UV-vis spectra for all 30 nm MOA-functionalized AuNPs before and after secondary ligand addition (A). No significant change in particle size is observed (average ± standard deviation) (B).

## Additional Notes on Washing Procedure

The washing procedure is critical to achieving accurate quantification of the ligands. Any ligands not bound to the AuNP surface must be washed away to give accurate quantification of ligands appended to the NP surface. As described in the experimental section of the main text, we wash all particles via centrifugation. After functionalization, particles are washed 6 times: twice with pH = 10 phosphate buffer, twice with water, and twice with $D_2O$. The buffer washes, including the overnight incubation in buffer, are used to disrupt hydrogen bonds that may form between the carboxylic acid-terminated ligands. For consistency, the same washing procedures with buffer, water, and $D_2O$ are used for all ligands.

All washing steps are conducted in 1.5 mL conical centrifuge tubes (4.0 cm tall (not including cap), with an inner diameter of 1.0 cm at the mid-section of the tube). Estimating from geometry and the lattice constant of gold, the rough molecular weight of a 13 nm AuNP ~ $1.3 \times 10^7$ Da, ~ 67,000 Au atoms and the rough molecular weight of a 30 nm AuNP ~ $1.6 \times 10^8$ Da, ~ 833,000 Au atoms. Both 13 nm AuNPs and 30 nm AuNPs are orders of magnitude larger than the ligands from which they are being separated. Last, due to the high extinction coefficient of the AuNP localized surface plasmon resonance (LSPR)[4], visual inspection is also a helpful guide for separation efficiency.

**Confirmation of PEGSH Identity**

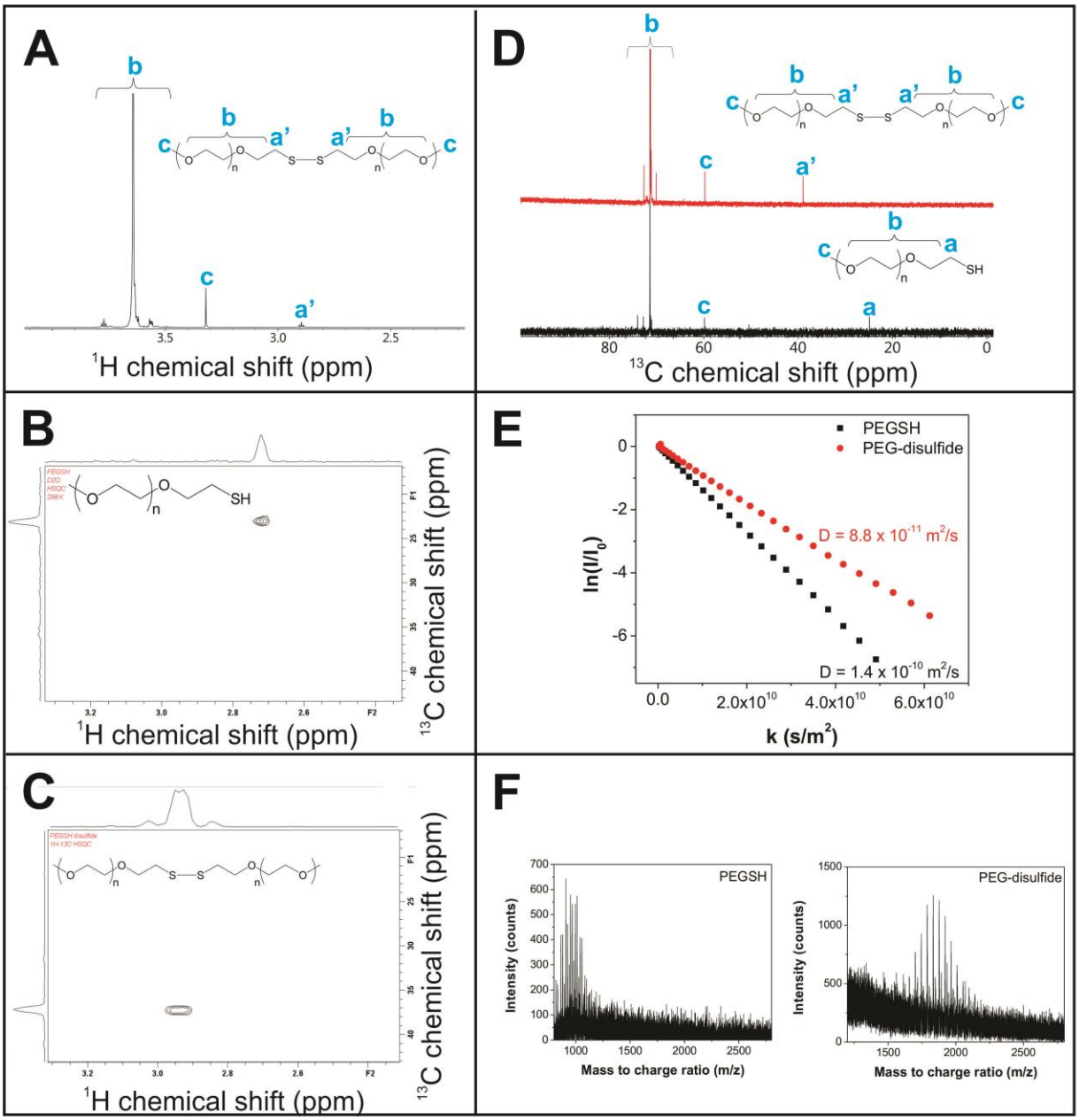


**Figure S30.** (A) 1D $^1$H NMR spectrum of PEG-disulfide. (B) $^1$H-$^{13}$C HSQC of PEGSH. (C) $^1$H-$^{13}$C HSQC of PEG-disulfide. (D) 1D $^{13}$C NMR overlay of PEGSH (black) with PEG-disulfide (red). (E) $^1$H diffusion decay curves of PEGSH (black) and PEG-disulfide (red). (F) MALDI-MS of PEGSH (left) and PEG-disulfide (right).

The disulfide analog of PEGSH was prepared according to a literature procedure.[5] The resulting PEG-disulfide was characterized with $^1$H NMR, $^{13}$C NMR, $^1$H-$^{13}$C heteronuclear single quantum coherence (HSQC) spectroscopy, $^1$H diffusion

ordered spectroscopy (DOSY), and matrix assisted laser desorption ionization mass spectrometry (MALDI-MS) and compared to the as-received PEGSH. The results and comparison are shown in Figure S30.

As a result of disulfide formation, a downfield shift of the $^{1}$H resonances adjacent to the sulfur is observed from ~2.7 ppm in PEGSH to ~2.9 ppm in PEG-disulfide (Figure S30A). From the $^{1}$H-$^{13}$C HSQC NMR and 1D $^{13}$C NMR analyses (Figure S30B-D), the $^{13}$C resonances adjacent to the sulfur in the PEGSH are characteristic of carbons adjacent to a thiol at ~25 ppm, whereas the $^{13}$C resonances adjacent to the sulfur in the PEG-disulfide are characteristic of carbons adjacent to a disulfide at ~39 ppm.

Further, apparent diffusion coefficients of both PEGSH and PEG-disulfide were measured using a stimulated echo bipolar pulsed field gradient sequence. Here, the diffusion coefficient is given as a function of NMR signal intensity (*I*) by a modified Stejskal-Tanner equation:[6]

$$I = I_0 exp\left(-(\gamma G\delta)^2\left(\Delta - \frac{\tau}{2} - \frac{\delta}{8}\right)\right)$$

where $I_0$ is the initial signal intensity, $\gamma$ is the gyromagnetic ratio of $^{1}$H, $G$ is the applied gradient strength, $\delta$ is the length of the gradient pulse, $\Delta$ is the diffusion time, $\tau$ is the time between bipolar gradient pulses, and $D$ is the apparent diffusion coefficient. Rearranging this equation gives:

$$\ln\left(\frac{I}{I_0}\right) = -(\gamma G\delta)^2\left(\Delta - \frac{\tau}{2} - \frac{\delta}{8}\right)D = -kD$$

A plot of $ln(I/I_0)$ vs $k$ allows for direct evaluation of the diffusion coefficient. The diffusion coefficients extracted from fitting $^{1}$H DOSY decay curves (Figure S30E) indicate that the PEG-disulfide exhibits a smaller apparent diffusion coefficient than PEGSH, indicating a larger size. The difference in diffusion coefficient is consistent with the difference in mass-to-charge ratio that is observed in MALDI-MS (Figure S30F). In the MALDI-MS of as-received PEGSH, there are no disulfides detected in the mass spectrum and the mass is consistent with 1 kDa. After reaction to form the PEG-disulfide analog, the MALDI-MS indicates that the mass-to-charge ratio has approximately doubled and corresponds to a disulfide.

References:

(1) Hanwell, M. D.; Curtis, D. E.; Lonie, D. C.; Vandermeersch, T.; Zurek, E.; Hutchison, G. R. *J. Cheminformatics* **2012**, *4*, 17.
(2) Rowland, R. S.; Taylor, R. *J. Phys. Chem.* **1996**, *100*, 7384.
(3) Harris, D. C. *Quantitative Chemical Analysis*; 7th ed.; W. H. Freeman and Company: New York, 2007.
(4) Jain, P. K.; Lee, K. S.; El-Sayed, I. H.; El-Sayed, M. A. *J. Phys. Chem. B* **2006**, *110*, 7238.
(5) Kirihara, M.; Asai, Y.; Ogawa, S.; Noguchi, T.; Hatano, A.; Hirai, Y. *Synthesis* **2007**, *2007*, 3286.
(6) Stejskal, E. O.; Tanner, J. E. *J. Chem. Phys.* **1965**, *42*, 288.